Atmos. Chem. Phys. Discuss., 5, 8285–8330, 2005
www.atmos-chem-phys.org/acpd/5/8285/
SRef-ID: 1680-7375/acpd/2005-5-8285
European Geosciences Union

Atmospheric Chemistry and Physics Discussions

An AeroCom initial assessment – optical properties in aerosol component modules of global models

S. Kinne[1], M. Schulz[2], C. Textor[2], S. Guibert[2], Y. Balkanski[2], S. E. Bauer[3], T. Berntsen[4], T. F. Berglen[4], O. Boucher[5,6], M. Chin[7], W. Collins[8], F. Dentener[9], T. Diehl[10], R. Easter[11], J. Feichter[1], D. Fillmore[8], S. Ghan[11], P. Ginoux[12], S. Gong[13], A. Grini[4], J. Hendricks[14], M. Herzog[12], L. Horowitz[12], I. Isaksen[4], T. Iversen[4], A. Kirkevåg[4], S. Kloster[1], D. Koch[3], J. E. Kristjansson[4], M. Krol[16], A. Lauer[14], J. F. Lamarque[8], G. Lesins[17], X. Liu[15], U. Lohmann[18], V. Montanaro[19], G. Myhre[4], J. Penner[15], G. Pitari[19], S. Reddy[12], O. Seland[4], P. Stier[1], T. Takemura[20], and X. Tie[8]

[1]Max-Planck-Institut für Meteorologie, Hamburg, Germany
[2]Laboratoire des Sciences du Climat et de l'environnement, Gif-sur-Yvette, France
[3]The Earth Institute at Columbia University, New York, NY, USA
[4]University of Oslo, Department of Geosciences, Oslo, Norway
[5]Laboratoire d'Optique Atmosph'erique, USTL/CNRS, Villeneuve d'Ascq, France
[6]Hadley Centre, Met Office, Exeter, UK
[7]NASA Goddard Space Flight Center, Greenbelt, MD, USA
[8]NCAR, Boulder, Colorado, USA

© 2005 Author(s). This work is licensed under a Creative Commons License.

[9] EC, Joint Research Centre, IES, Climate Change Unit, Ispra, Italy
[10] Goddard Earth Sciences and Technology Center, UMBC, Baltimore, MD, USA
[11] Batelle, Pacific Northwest National Laboratory, Richland, USA
[12] NOAA, Geophysical Fluid Dynamics Laboratory, Princeton, NJ, USA
[13] ARQM Meteorological Service Canada, Toronto, Canada
[14] DLR, Institut für Physik der Atmosphäre, Oberpfaffenhofen, Germany
[15] University of Michigan, Ann Arbor, MI, USA
[16] Institute for Marine and Atmospheric Research Utrecht (IMAU) Utrecht, The Netherlands
[17] Dalhousie University, Halifax, Canada
[18] ETH Zürich, Switzerland
[19] Universita degli Studi L'Aquila, L'Aquila, Italy
[20] Kyushu University, Fukuoka, Japan

Correspondence to: S. Kinne (kinne@dkrz.de)

Received: 25 May 2005 – Accepted: 12 July 2005 – Published: 8 September 2005

Abstract

The AeroCom exercise diagnoses multi-component aerosol modules in global modeling. In an initial assessment simulated global distributions for mass and mid-visible aerosol optical thickness (aot) were compared among 20 different modules. Model diversity was also explored in the context of previous comparisons. For the component combined aot general agreement has improved for the annual global mean. At 0.11 to 0.14, simulated aot values are at the lower end of global averages suggested by remote sensing from ground (AERONET ca. 0.135) and space (satellite composite ca. 0.15). More detailed comparisons, however, reveal that larger differences in regional distribution and significant differences in compositional mixture remain. Of particular concern are large model diversities for contributions by dust and carbonaceous aerosol, because they lead to significant uncertainty in aerosol absorption (aab). Since aot and aab, both, influence the aerosol impact on the radiative energy-balance, the aerosol (direct) forcing uncertainty in modeling is larger than differences in aot might suggest. New diagnostic approaches are proposed to trace model differences in terms of aerosol processing and transport: These include the prescription of common input (e.g. amount, size and injection of aerosol component emissions) and the use of observational capabilities from ground (e.g. measurements networks) or space (e.g. correlations between aerosol and clouds).

1 Introduction

Aerosol is one of the key properties in simulations of the Earth's climate. Model-derived estimates of anthropogenic influences remain highly uncertain (IPCC, Houghton et al., 2001) in large part due to an inadequate representation of aerosol. Aerosol originates from diverse sources. Source-strength varies by region and often by season. and aerosol has a short lifetime on the order of a few days. Thus, concentration, size, composition, shape, water uptake and altitude of aerosol are highly variable in space and

time. In recent years worldwide parallel efforts have resulted in new approaches for aerosol representation and aerosol processing. Common to most of these approaches is a discrimination of aerosol in at least five aerosol components: sulfate, organic carbon, black carbon, mineral dust and sea-salt. The separate processing of these aerosol types added complexity and required new assumptions. To test the skill of new aerosol modules beyond selective comparisons to processed remote sensing data, modeling groups joined the aerosol module evaluation effort called AeroCom. This paper introduces goals and activities of AeroCom and summarizes aspects of diversity in global aerosol modeling as of 2005 – also intended to establish a benchmark on which to measure improvements of future modeling efforts. The paper presents results with regard to optical properties from the first AeroCom experiment (A), which represents the models "as they are". More details on "Experiment A" model diversity, including a comprehensive analysis of budgets for aerosol mass and processes are given in companion paper by Textor et al. (2005).

2 AeroCom

AeroCom intends to document differences of aerosol component modules of global models and to assemble data-sets for model evaluations. Overall goals are (1) the identification of weaknesses of any particular model and of modeling aspects in general and (2) an assessment of actual uncertainties for aerosol optical properties and for the associated radiative forcing. AeroCom is open to any global modeling group with detailed aerosol modules and encourages their participation. AeroCom also seeks the participation of groups, which provide data-sets on aerosol properties. AeroCom assists in data quality assessments, data combination and in data extension to the temporal and spatial scales of global modeling.

In order to perform model-intercomparisons and comparisons to measurement based data AeroCom requests detailed model-output and provides a graphical evaluation environment for participants through its website http://nansen.ipsl.jussieu.fr/

AEROCOM. The website also lists the presentations of the initial three workshops held at Paris (June 2003), Ispra (March 2004) and New York (December 2004). These regular workshops are organized (1) to coordinate activities, (2) to encourage interactions among modeling groups and (3) to engage communications between modeling and measurement groups on data-needs and data-quality.

A common data-protocol has been established and was distributed to the participants in spring 2003 (see also AeroCom website). Model-output requests are primarily tailored to allow budget analysis and comparisons to available data. Additional requests are included to explore details on model specific assumptions and processes, such as size distribution, surface wind speed, precipitation, aerosol water or daily cloud fraction and radiative forcing. Several consecutive experiments have been proposed to explore diversity in global modeling on the path towards improved aerosol direct and aerosol indirect forcing estimates. At this stage four experiments have been defined and output requests are summarized in Table 1.

Experiment A: modelers are asked to run models in their standard configuration. Model output is requested either from climatological runs (averaged for 3–10 years) or from simulations constrained by the meteorological fields for the years 1996, 1997, 2000 and 2001, with preference on 2000.

Experiment B: modelers are asked to use AeroCom's prescribed emission sources for the year 2000 and (when possible) meteorological fields for the year 2000. The additional request to extend simulations into the first two months of the year 2001 will allow comparison to TERRA satellite data for a complete yearly cycle.

Experiment Pre: modelers are asked to repeat Experiment B now using AeroCom's prescribed emission sources for the year 1750 rather than for the 2000. Radiative forcing calculations are asked with priority for the experiments B and PRE.

Experiment Indi: modelers are asked to conduct model-sensitivity studies to better quantify uncertainties regarding the aerosol impact on the hydrological cycle with particular constraints to baseline conditions (e.g. aerosol mass and/or size), parameterizations (e.g. aerosol impact on the cloud droplet concentration or precipitation

efficiency) or effects (e.g. aerosol heating).

A future intention of the AEROCOM initiative is that the least constrained "Experiment A" can be revisited to quantify improvements by future efforts in aerosol modeling. More insights on differences in aerosol modeling are expected from "Experiment B", where model input is harmonized in terms of aerosol emissions for the year 2000. "Experiment Pre" is the counterpart to "Experiment B", as it provides the reference in estimates of anthropogenic contributions and associated forcing. The prescribed AeroCom (component) emissions for "Experiment B" and "Experiment Pre" can be downloaded at ftp://ftp.ei.jrc.it/pub/Aerocom/. The choices made to arrive at a harmonized emission data set for all major aerosol components are explained in more detail in Dentener et al. (2005)[1]. "Experiment Indi" is different in that it investigates the sensitivity of modeling and the model diversity of processes and parameterizations essential to estimates of the aerosol indirect effect. Details can be found under http://nansen.ipsl.jussieu.fr/AEROCOM/INDIRECT/indirect_protocol.html.

3 Results

The database consists now of results from twenty modeling groups. Table 2 lists the 16 "Experiment A" AeroCom participants, who submitted full datasets and 4 contributors, who submitted at an earlier stage (e.g. in Kinne et al., 2003) or provided only partial information.

In this paper only results of "Experiment A" are explored, preferably those for the year 2000. Submissions to the three other experiments at this stage are incomplete or in preparation. Simulated properties for aerosol optical depth (aot), aerosol absorption (aab) are compared – with a focus on global measurements from ground-based

[1] Dentener, F., Kinne, S., Bonds, T., Boucher, O., Cofala, J., Generoso, S., Ginoux, P., Gong, S., Hoelzemann, J., Ito, A., Marelli, L., Putaud, J.-P., Textor, C., and Schulz, M.: Emissions of primary aerosol and precursor gases in the years 2000 and 1750: prescribed data-sets for AeroCom, MPI reports, in preparation, 2005.

networks and satellites. In addition, differences in aerosol mass extinction efficiency (mee), the mass to aot conversion factor, are explored to illustrate model-diversity of assumptions for aerosol size and humidification.

Simulated global annual averages are addressed first to provide a general overview. Then more insights are provided from regional differences. Finally, seasonality issues are addressed.

3.1 Global annual averages

When validating aerosol module simulations on a global scale, it has become customary to compare simulated annual global aot values to those obtained from remote sensing. Comparisons among model simulations for (the annual and globally averaged) for the mid-visible aot (at 550 nm) are presented in Fig. 1. This figure illustrates also how model simulations have changed from the work of Kinne et al. (2003) to the present. Figure 1 also includes data from remote sensing. Since all remote sensing data are spatially incomplete, a correction was applied, based on the bias such sub-sampling would introduce to aot data of the model median. The upper panel presents global averages from TOMS, MISR, MODIS, AVHRR and POLDER retrievals (corresponding global distributions for aot are presented later in section 3). Table 3 summarizes contributing time-periods, retrieval references and known biases (a comparison of regional averages is presented later in Sect. 3.3). Some of these biases were also discussed in recent papers (Myhre et al., 2005; Jeong and Zi, 2005). The lower panel only displays two remote sensing references: A satellite composite (S*), which combines the strength of individual retrievals and an estimate based on statistics at AERONET ground sites.

The lower panel of Fig. 1 indicates the two recommended remote sensing based references for the global annual aot at 0.135 (Ae – AERONET) and at 0.151 (S* – satellite composite). The composite value (S*) is based on monthly $3^{\circ}\times3^{\circ}$ longitude/latitude monthly averages, where preference is given to year 2000 data. Over land preference is given to MISR over TOMS, except in the central tropics, where MODIS is preferred

over MISR. Over oceans MODIS is preferred over AVHRR-1ch, whereas this order in reversed at mid-(to high) latitudes. The AERONET value (Ae) is based on monthly statistics at all (ca. 120) ground-sites, which provided quality data for the year 2000. The site density of the land-sites is highest for the US and Europe, but very weak for Northern Africa and Asia (http://aeronet.gsfc.nasa.gov).

Figure 1 shows that the agreement among models improved for the global annual aot during the last three years. In 2005 the simulated aot (the total aot of all component combined) on a global annual basis in most models remains within 15% of a value of 0.125. This represents a marked improvement over the initial comparison of eight models in 2002. Most simulated global averages now agree well to both consolidated high-quality data from remote sensing (Ae and S* in the lower panel of Fig. 1). This raises the question, if consistency in aerosol processing improved in a similar fashion or if the better agreement largely reflects adjustments to satisfy tighter constraints by remote sensing.

All participating global aerosol modules in this comparison distinguish between five different aerosol components: sulfate (SU), black carbon (BC), particulate organic matter (POM), dust (DU) and sea-salt (SS). All models simulate (generally from emission inventories) global fields of aerosol component mass. Then this mass is converted into (spectrally dependent optical) properties of) aot and absorption, from which eventually estimates for the aerosol impact on the energy balance are derived (commonly quantified by the radiative forcing). Figure 2 illustrates these successive processing steps in aerosol modeling.

The simulated (aerosol) radiative forcing depends on both: aot and absorption as illustrated in Fig. 2. Thus, the commonly tested aot agreement (to data) alone cannot guarantee accurate estimates in radiative forcing. It is possible that the agreement to now available higher quality aot data from remote sensing (see Fig. 1) improved so quickly, because each model has enough freedom for any aerosol component to adjust data on (1) emission, (2) processes affecting aerosol lifetime and (3) aerosol size – also via aerosol water uptake. This suspicion is certainly supported by a comparison

of aot contributions from the individual sub-components. Figure 3 reveals large model differences in compositional mixture (which has not changed since the last assessment in Kinne et al., 2003). It also demonstrates that the agreement for the sum of all components, which was presented in Fig. 1 is a poor measure for overall model skill and model diversity. Model diversity for each of the five component aot contributions individually is significantly larger than for the combined total aot. This is also quantified in Table 4, where annual global averages – on a component basis – are compared among all aerosol modules. In the right-most column of Table 4, the diversity for just the 16 aerosol modules of the AeroCom exercise is summarized by total diversity (TD) and in brackets by central diversity (CD): both TD and CD are defined by the ratio between the largest and smallest average. Thus, a value of one corresponds to perfect agreement and any amount larger than one is the adopted measure of diversity. TD refers to all models, whereas CD refers only to the central 2/3 of all models – as extremes in modeling for CD are excluded.

For aot, the CD of individual components contributions is between 2.0 and 2.7. This is three to six times larger than for the component combined total of 1.3 (which was illustrated by model comparison for 2005 in Fig. 1). The largest component CDs for aot are associated with black carbon, dust and sea-salt. CDs for aot-to-mass conversions (mass-extinction-efficiency) indicate (see Table 4) that for sea-salt and dust differences in aerosol size are a major reason for their aot diversity. Aerosol size is not only influenced by assumptions to primary emissions but also by the permitted water uptake, which is controlled by assumptions to component humidification and local ambient humidity. Table 4 indicates that on a global annual basis the simulated aerosol water mass shows strong diversity and aerosol water mass is (at least) comparable to the aerosol dry mass of all sub-components combined. Thus, for the hydrophilic components of sea-salt and sulfate larger model diversities are expected for aot than for dry mass. For global sea-salt CDs, however, this trend is reversed. A possible explanation is the transport of larger sea salt particles in some models, which creates larger diversity near sources more so for mass than for aot. A contributing factor is also

the large sea-salt mass diversity over continents (see discussions in the next section and the presentation of diversity fields in Fig. 4). This illustrates that even regions with significant lower concentrations can distort the global average and that the reliance on global averages can be misleading. Thus, local diversity fields are explored next.

3.2 Annual fields

Given the short-lived nature of aerosol, evaluations at sufficient resolution in time and space will allow more useful insights into issues of aerosol global modeling. To extend the model diversity assessments of Table 4, local CDs for 24 annual fields are presented in Fig. 4. All models were interpolated to the same horizontal resolution of $1^{\circ}\times1^{\circ}$ latitude/longitude. At each grid point all models were ranked according to the simulated magnitude into a probability distribution function (PDF). The ratio between the 83% and the 17% values of the PDF (such that extremes in modeling are ignored) define the CDs in Fig. 4. It can be seen that model diversity usually increases towards remote regions, largely due to differences in transport and/or aerosol processing (e.g. removal). However, diversity has to be judged also in the context of the absolute concentration, as larger diversities are less meaningful in regions of overall low concentrations. Global fields of the model median (the 50% value of the PDF) are presented in figures of the Appendix, where Fig. A1 corresponds to Fig. 4.

Model diversity is usually larger over land than over oceans for total dry mass and total aot. The largest differences occur in central Asia and extend eastwards to western regions of North America. Sub-component diversity is usually stronger, but component diversity patterns differ. For sulfate the diversity for aot is increased over mass diversity at low latitude land regions and in the continental outflow regions. Large model diversity for aerosol water may provide an explanation. For organic and black carbon the diversities are usually larger than for sulfate. Particular large are carbon diversities over some oceanic regions. This location over the ocean for the rather insoluble organic particles suggests model differences in transport and removal processes which affect the transport to remote regions. As differences in transport strongly contribute to model

diversity, it is not surprising that for dust, whose global distributions are largely defined by transport, display larger diversities away from dust source regions. The fact that dust diversity (and sea-salt diversity over oceans) for aot is significantly smaller than for mass could indicate deliberate choices by modelers for size with the goal to match expectations. However, it should be pointed out, that different cut-off assumptions for the largest dust and sea-salt sizes create mechanically larger diversity for mass than for aot (the largest particles contribute a lot to mass but little to aot). The size-diversity for dust and sea-salt is also demonstrated in larger diversities for mass-to-aot conversion factors (the r- panels in the third column of Fig. 4), compared to carbon or sulfate species. Also, the largest model diversity for the Angstrom parameter (aerosol size) occurs in regions, where dust (Northern Africa and Asia) and sea-salt (southern mid-latitudes) are the dominant components.

A comparison of the panels in the upper corners of Fig. 4 illustrates that diversity for aerosol absorption is significantly larger than for aerosol optical thickness. This indicates that reduced uncertainties in aerosol direct forcing require primarily improvements to the characterization of the local (or regional) aerosol composition. Larger diversities for absorption occur towards remote regions. This suggests that aerosol processing during long-range transport is a key issue for reductions of model diversity. Emissions which dominate the diversity near the sources over land seem to be more homogeneous in models, probably because similar emission inventories are used by different modeling groups.

3.3 Comparisons to observational data

Although model diversity is of interest, it is not necessarily a measure of the real uncertainty. Similar assumptions or approaches in modeling can overshadow real uncertainties, as for example in the case of moderate diversity found for organic carbon (mass) despite large uncertainties for its emission factors, secondary production, humidification and absorption.

Model diversity is of limited value without quality reference observations, which from

now on is referred to as data, for simplicity. Unfortunately, reference data are only available for a few (and often integrated) properties. And even if data exist, they usually suffer from limitations to (often poorly defined) accuracy and from restrictions of spatial and/or temporal nature. Subsequent comparisons focus on two properties that are critical in the context of aerosol radiative forcing: mid-visible values for aot and aab (absorption-aot, which is the aot fraction linked to absorption). The first data reference is provided by the AERONET robotic sun-/sky-photometer network (Holben et al., 1998). Aot data are sampled at high accuracy, whereas aab samples are only reliable at, larger aot (Dubovik et al., 2002). A major concern is the potential for local biases of AERONET data (e.g. by local pollution) which cannot be resolved in coarse gridded (e.g. 200*200 km) model simulations. Thus, comparisons were limited at this stage to 12 sites, where local biases are believed to be small. Site details, which are summarized in Table 5, indicate that the selected sites cover a variety of aerosol types and regions.

The second data reference is established by a satellite aot retrieval composite (S*). Its annual average aot field is compared in Fig. 5 to aot-retrievals of individual sensor. The choices of individual retrievals contributing to the aot retrieval composite (S*) are based on regional comparisons to regional AERONET. Annual aot averages of individual remote sensing efforts, of the retrieval composite (S*) and of the model median for the regions of Fig. 7 (meridional sections associated with land, coastal and ocean surfaces) are compared in Table 6.

3.3.1 Global

For a first impression on model performance in general, relative aot deviations of the model median to the satellite composite (S* in Fig. 5) are presented on a monthly basis in Fig. 6. Values of +1/−1 indicate over-/under-estimates of 100%, with respect to the satellite reference.

Most noticeable are model overestimates for Europe during the summer months. This trend even extends during the late summer into Northern Asia. Other median

model biases are the too early biomass burning season in South America, too much dust in Northern Africa during the winter season, and aot underestimates in tropical regions. Given that satellite retrievals over oceans are less uncertain than over land, the large discrepancy to modeling over tropical oceans is puzzling. More quantitative comparisons for regions of Fig. 7 are given in Table 6. Table 6 list the regional averages of the satellite composite (S*) and compares them to spatial adjusted AERONET averages (Ae) and to the median in global modeling (med). (Here again, spatial adjustments were based on model median data, as the average based on data associated spatial sub-sampling is compared to the average using all data in the region of choice).

3.3.2 Regional and local

Comparisons in this section are illustrated in a similar format. For selected locations and regions, monthly averages are presented in a clock-hourly sense (12–1: January, ..., 11–12: December). Purple (sectional) disks indicate monthly data at a magnitude according to the disk-size in the lower right. Following the same magnitude scale, green lines illustrate the mean in modeling, while blue and yellow sections indicate ranges between maximum and minimum in modeling in reference to all models (TD) and central-2/3 models (CD). Disagreement is apparent, when the yellow range of modeling is completely within or outside the purple area of the data.

Aot data

Simulated aot data are compared locally in Fig. 8 at 12 sites to AERONET statistics and regionally in Fig. 9 for 21 (highlighted) regions to the satellite retrieval composite.

The two main model biases common to both data-references are (1) too large aots over Europe and (2) a too early biomass burning season in South America. Other modeling biases with respect to the two reference data do not match: AERONET suggests that models (1) underestimate the strength of the tropical biomass burning season, (2) overestimate Eastern Asia contributions in off-dust seasons and (3) overestimate

during US winters. The satellite composite suggests that (1) simulations are too low over tropical oceans, (2) the seasonality peak for central Asia is reversed and (3) dust transport from Asia to North America is too low. In light of retrieval issues, there is less confidence in biases to satellite over land. However, aot underestimates of most models to MODIS over tropical oceans are significant. Unfortunately, ground data are too spare to clarify this issue.

The intra-regional standard deviation for aot is compared in Fig. 10. Dust and dust-outflow regions display the largest aot variability in modeling. Common to most models is a stronger variability over (1) central Asia during summer and fall (related to dust), (2) Eastern Asia, (3) Northern Africa and (4) Europe, during winters. Variability is weaker over (1) North America and (2) Southern Africa during the biomass season. Most models display significantly stronger inter-regional variability for monthly aot averages than the satellite reference, although discrepancies are largest in regions, where retrievals are difficult and often sparse to start with.

Absorption data

Aerosol absorption is best quantified by the product of aot and co-single scattering albedo, the absorption aot (aab). Local comparisons at AERONET sites are given in Fig. 11.

Models overestimate absorption strength in the Eastern US and in the Mid-East. On the other hand tropical biomass absorption strength is underestimated and the peak occurs too early in South America. Notable are disagreements for the central African AERONET site, where the simulated (biomass) absorption at year's end is too large, but too weak in the opposite season.

Values for aab were only provided by about half of the models. To capture the diversity for the absorption potential involving all models, a different approach was selected by deriving the mid-visible (.55 μm) imaginary part of the Refractive Index (RFi) from simulated component dry mass contributions for all models. First, assumed component

RFi values (0.0015 for dust, 0.03 for particulate organic matter, 0.6 for black carbon and zero for all other components) were multiplied by corresponding fractional volume weights to yield the dry RFi of the mixtures. Then, for the actual RFi, the wet RFi of the mixture, the non-absorbing volume fraction of aerosol water was added, where water amounts of the model median were applied. Regional and monthly RFi statistics of AeroCom models are presented in Fig. 12.

The modeled absorption potential is strongest in the tropical biomass regions, with a seasonal peak which occurs prior to the seasonal peak for aot. Also the absorption potential is larger for Europe than for Asia or North America. Relatively low is the absorption potential for the Eastern US. Lowest values were modeled for ocean regions away from sources. However, the main point is that there is significant model diversity for the absorption potential as a consequence from large difference in aerosol composition. This diversity is at least as large as the diversity for aot (see also Fig. 4).

3.3.3 Discussion

Larger values for aot over Europe are probably related to emission overestimates in older inventories, which were generally used in modeling. Similarly, the too early biomass burning season in South America strongly suggests the use of incorrect emission data. The biases found here provide an additional motivation for the AeroCom "Experiment B", where updated emissions are required to be used as model input. More difficult are explanations for aot discrepancy in remote regions of tropical and Southern Hemisphere oceans between modeling and satellite retrievals, which are believed to have good cloud-detection capabilities, such as MODIS. Although absolute aot differences generally do not exceed 0.1, relative differences often exceed a factor of two. It remains unclear, if deviations are to be blamed on modeling (e.g. transport) or retrieval error (e.g. cloud contamination). Unfortunately, surface observations currently are too sparse to clarify this issue in the southern ocean regions.

In terms of aerosol absorption, it should be pointed out, that there are large differences in aerosol composition among models. The absorption potential of sub-

components differs strongly. Thus, significant absorption differences among models are expected. However, only a few models provided data on single scattering albedo (ω_0), as a measure of specific absorption, from (less clear) assumptions to component absorption or water uptake. Thus, to demonstrate diversity of all models, fixed values for component absorption and water uptake (of the model median) were assumed and RFi for individual models were derived based on volume weights (using data on component mass). Regional comparisons for RFi were presented in Fig. 12 and demonstrate the (potentially – due to fixed values) large model diversity for absorption. (Further RFi conversion into ω_0 (RFi is proportional to [1-ω_0]) failed, because this conversion is size dependent (e.g. coarser aerosol is associated with larger values for [1-ω_0] for the same RFi). For models that provided values for ω_0, simulated absorption strength can be compared to local statistics of AERONET, from the ratio of aab (Fig. 11) and aot (Fig. 8). Based on these ratios, models underestimate the specific aerosol absorption over industrial areas in North America and Europe (only very large aot overestimates lead to total absorption overestimates in Europe). A location of the AERONET sites near sources of pollution and the expected bias to more absorption at low aot values in AERONET radiance data inversion (e.g. see the Tahiti site in Fig. 11) are potential explanations, but underestimates for black carbon emissions in the models cannot be ruled out either.

4 Conclusion

Comparisons of aerosol properties simulated by newly developed aerosol component modules for/in global modeling have demonstrated a surprising good agreement for the annual global aerosol optical depth, quite in agreement with recent efforts to obtain improved remote sensing observations. However, the notion that uncertainties for the (aerosol) direct forcing have reduced in a similar way are premature. This aot agreement is not supported on a sub-component level for aerosol optical depth and even less for component aerosol dry mass and aerosol water from which these (component)

aerosol optical depths are derived. The large differences in compositional mixture for aerosol dry mass and water uptake affect aerosol absorption. Thus, despite general agreement for aot, strong diversity for aerosol absorption will introduce large uncertainties to the aerosol associated solar radiative (direct) forcing. In particular, uncertainties for the climate forcing term (the changes for the solar energy balance at the top of the atmosphere) will be large, because this term represents a difference of two values with similar magnitude but opposite in sign (a loss term due to solar scattering and a gain term due to aerosol absorption). To summarize: Good agreement for total aot (-fields) does not guarantee good agreement for aerosol forcing and diversity for total aot among models is an insufficient measure for forcing diversity.

In the initial AeroCom "Experiment A" comparisons, models were allowed the input of their choice. Diversity patterns are large enough, to recommend further investigations into modeling differences. Better constraints to input in "Experiment B" and "Experiment Pre" should enhance current capabilities to reveal strength and weaknesses on issues associated with aerosol processing and aerosol transport. The AeroCom effort has developed a transparent strategy to document overall model diversity and individual model bias to a multitude of observational data. Further progress for model evaluations is expected in the near future from more capable data sensors (e.g. active remote sensing from space for vertical profiles [A-train]), higher temporal and spatial resolution (e.g. more capable geostationary satellites [MSG]) and new and improved ground (e.g. AERONET) and in-situ (e.g. commercial airlines) networks. On the other hand, as aerosol modules in global modeling strive to include more processes and feedbacks, the complexity of aerosol modules will increase, and so will the need for more specific measurement detail.

Appendix

Global reference fields for aerosol properties from modeling

Given the short lifetime of quite different types and processes of aerosol, there is a need for reliable references on regional and seasonal distributions of aerosol properties in the global context. Observational data-sets (e.g. from remote sensing) should be the first choice. But measurements are only available for a few often integrated properties. And even then these data are usually spatial and temporal restricted and/or suffer from severe accuracy limitations.

Aerosol modules in global modeling can provide complete and consistent global fields for all aerosol properties. Rather than relying on one single module, here the whole suite of all 16 modules participating in the AeroCom is the basis to the reference data on aerosol properties. The data presented below represent the model median values (at a common 1*1 degree latitude/longitude spatial resolution). The median rather than the average was chosen in order to avoid contaminations by extreme behavior of any particular model.

Annual average fields for 24 aerosol properties are presented in Fig. A1. Each field to its left is identified by a label and a maximum value for the generic linear scale. The first column displays the mid-visible aerosol optical depth (a) and contributions by the five sub-components of sulfate (-S), particulate organic matter (-O), black carbon (-B), sea-salt (-N) and dust (-D). The second column shows the corresponding distribution for aerosol (column) dry mass (m) and the five subcomponents (in units of g/m2). Additional fields, addressing the aspect of aerosol mass are the fields for the organic BC/POM mass-ratio (cr) and for aerosol water (W). Note, that in most regions aerosol water mass exceeds aerosol dry mass. In the third column, sub-component information of the first two columns is combined, by displaying the mass-to-aot multiplicator (r) fields, demonstrating the one order of magnitude larger mass extinction efficiency for sulfate and carbon as compared to sea-salt or dust. This is largely related to aerosol size, whose variations are illustrated by the fields for Angstrom parameter (An) and

the fine mode-fractions (fractional contributions by aerosol size smaller than 1 μm) for visible attenuation or aot (af) and mass (mf). Finally, aerosol absorption is illustrated by the two top panels in the 4th column. The single-scattering albedo field (w0) illustrates the (mid-visible/.55 μm) absorption potential, whereas the absorption aot (ab), the product of co-single scattering albedo and aot, represents a measure for the total (mid-visible/.55 μm) absorption.

Since seasonal variations are often of interest, in addition monthly averages are presented for selected properties of Fig. A1. To illustrate the impact on visual attenuation, Fig. A2 compares monthly data for the mid-visible aerosol optical depth. To demonstrate absorption potential, Fig. A3 shows monthly aerosol single scattering albedos. To indicate aerosol size, Fig. A4 presents monthly patterns for the Angstrom parameter. Values above 1 indicate a dominant attenuation by sub-micron aerosol sizes, whereas at values smaller than 0.5 super-micron sizes dominante attenuation. Figure A5 compares monthly aerosol mass patterns, clearly showing the higher sensitivity to larger aerosol sizes as compared to aot (attenuation) and Fig. A6 finally combines information of Figs. A2 and A3 to total absorption fields.

Acknowledgements. The data comparisons would not have been possible without the support by the various satellite retrievals groups and data-centers in the US and the support of the AERONET community. In particular, we like to acknowledge the support by the AERONET staff lead by B. Holben in the US and P. Goloub in Europe and we thank the site managers of the 12 AERONET sites, whose data were used in local comparisons. We also acknowledge access and assessment help for the many global aerosol data-sets from satellite retrievals, including O. Torres for the TOMS data, L. Remer for the MODIS data, R. Kahn and J. Martonchik for the MISR data, J.-L. Deuzé and P. Lallart for the POLDER data, I. Geogdzhayev and M. Mishchenko for the 2-channel AVHRR data and A. Ignatov for the 1-channel AVHRR data. Also acknowledged is the support for this study by the EU PHOENICS project.

References

Deuzé, J. L., Herman, M., and Goloub, P.: Characterization of aerosols over ocean from POLDER/ADEOS-1, Geophys. Res. Lett., 26, 1421–1424, 1999.

Deuzé, J. L., Bréon, F. M., Devaux, C., Goloub, P., Herman, M., Lafrance, B., Maignan, F., Marchand, A., Nadal, F., Perry, G., and Tanré, D.: Remote sensing of aerosol over land surfaces from POLDER/ADEOS-1 polarized measurements, J. Geophys. Res., 106, 4912–4926, 2001.

Dubovik, O. and King, M.: A flexible inversion algorithm for the retrieval of aerosol optical properties from sun and sky radiance measurements, J. Geophys. Res., 105, 20 673–20 696, 2000.

Geogdzhyev, I., Mishchenko, M., Rossow, W., Cairns, B., and Lacis, A.: Global 2-channel AVHRR retrieval of aerosol properties over the ocean for the period of NOAA-9 observations and preliminary retrievals using NOAA-7 and NOAA-11 data, J. Atmos. Sci., 59, 262–278, 2002.

Ignatov, A. and Nalli, N.: Aerosol retrievals from multi-satellite AVHRR pathfinder (PATMOS) data-set for correcting remotely sensed sea surface temperature, J. Atm. Ocean. Tech., 19, 1986–2008, 2002.

Holben, B., Eck, T., Slutsker, I., Tanre, D., Buis, J., Vermote, E., Reagan, J., Kaufman, Y., Nakajima, T., Lavenau, F., Jankowiak, I., and Smirnov, A.: AERONET, a federated instrument network and data-archive for aerosol characterization, Rem. Sens. Environ., 66, 1–66, 1998.

Houghton, J., Ding, Y., Griggs, D., Noguer, M., van der Linden, P., Dai, X., Maskell, K., Johnson, C., Meira Filho, L., Bruce, J., Lee, H., Callander, B., Haites, E., Harris, N., and Maskell, K.: Climate Change 2001, The Scientific Basis, an evaluation of the IPCC (International Panel on Climate Change), Cambridge University Press, New York, 2001.

Jeong, M. J. and Li, Z.: Quality, comparability and synergy analyses of global aerosol products, Part 1: AVHRR and TOMS, J. Geophys. Res., 110, D10S08, doi:10.1029/2004JD004647, 2005.

Kahn, R., Banerjee, P., McDonald, D., and Diner, D. J.: Sensitivity of multi-angle imaging to aerosol optical depth and to pure particle size distribution and composition over ocean, J. Geophys. Res., 103, 32 195–32 213, 1998.

Kaufman, Y., Tanré, D., Remer, L., Vermote, E., Chu, D., and Holben, B.: Operational remote

sensing of tropospheric aerosol over the land from EOS-MODIS, J. Geophys. Res., 102, 17 051–17 061, 1997.

Kinne, S., Lohmann, U., Feichter, J., Timmreck, C., Schulz, M., Ghan, S., Easter, R., Chin, M., Ginoux, P., Takemura, T., Tegen, I., Koch, D., Herzog, M., Penner, J., Pitari, G., Holben, B., Eck, T., Smirnov, A., Dubovik, O., Slutsker, I., Tanré, D., Torres, O., Mishchenko, M., Geogdzhayev, I., Chu, D. A., and Kaufman, Y.: Monthly Averages of Aerosol Properties: A Global comparison among models, satellite data and AERONET ground data, J. Geophys. Res., 108, 4634, doi:10.1029/2001JD001253, 2003.

Martonchik, J. V., Diner, D. J., Kahn, R. A., Ackerman, T. P., Verstraete, M. E., Pinty, B., and Gordon, H. R.: Techniques for the retreival of aerosol properties over land and ocean using multi-angle imaging, IEEE Trans. Geosci. Remt. Sensing, 36, 1212–1227, 1998.

Myhre, G., Stordal, F., Johnsrud, M., Diner, D. J., Geogdzhayev, I., Haywood, J. M., Holben, B., Holzer-Popp, T., Ignatov, A., Kahn, R., Kaufman, Y., Loeb, N., Martonchik, J., Mishchenko, M., Nalli, N., Remer, L., Schroeter-Homscheid, M., Tanré, D., Torres, O., and Wang, M.: Intercomparison of satellite retreived aerosol optical depth over ocean during the period September 1997 to December 2000, Atmos. Chem. Phys., 5, 1697–1719, 2005, SRef-ID: 1680-7324/acp/2005-5-1697.

Tanré, D., Kaufman, Y. J., Herman, M., and Mattoo, S.: Remote Sensing of aerosol properties over ocean using the MODIS/EOS spectral radiances, J. Geophys. Res., 102, 16 971–16 988, 1997.

Textor, C., Schulz, M., Guibert, S., Kinne, S., Bauer, S., Balkanski, Y., Berntsen, T., Berglen, T., Boucher, O., Chin, M., Dentener, F., Diehl, T., Feichter, H., Fillmore, D., Ghan, S., Ginoux, P., Gong, S., Grini, A., Hendricks, J., Horrowitz, L., Isaksen, I., Iversen, T., Kirkevag, A., Koch, D., Kristjansson, J. E., Krol, M., Lauer, A., Lamarque, J. F., Liu, X., Montanaro, V., Myhre, G., Penner, J., Pitari, G., Reddy, S., Seland, O., Stier, P., Takemura, T., and Tie, X.: Analysis and quantification of the diversities of aerosol life cycles within AeroCom, Atmos. Chem. Phys. Discuss., 5, 8331–8420, 2005, SRef-ID: 1680-7375/acpd/2005-5-8331.

Torres, O., Barthia, P. K., Herman, J. R., Sinyuk, A., Ginoux, P., and Holben, B.: A long-term record of aerosol optical depth from TOMS observationsand comparisons to AERONET measurements, J. Atmos. Sci., 59, 398–413, 2002.

Table 1. Mandatory (X) and optional (O) output requests for the initial four experiments.

Specification	subpage on AeroCom web	Exp A	Exp B	Exp Pre	Exp Indi
Daily	/protocol_daily.html	X	X		
Monthly	/protocol_monthly.html	X	X	X	
Forcing	/protocol_forcing.html	X	X	X	
indirect – basic	/protocol_indirectforcing.html		X	X	O
indirect – full	/INDIRECT/indirect_protocol.html				X

Table 2. Global models with aerosol component modules participating in model assessments.

	AeroCom ID	Model	Type	res (deg)	lev	period	data	Authors
LO	*LOA*	LMDzT at LOA	GCM	3.8 / 2.5	19	yr 2000	all	Reddy / Boucher
LS	*LSCE*	LMDzT at LSCE	GCM	3.8 / 2.5	19	yr 2000	all	Schulz / Balkanski
UL	*ULAQ*	ULAQat L'Aquila	CTM	22.5 / 10	26	yr 2000	all	Pitari / Montanaro
SP	*KYU*	SPRINTARS at KYU	GCM	1.1 / 1.1	20	yr 2000	all	Takemura
CT	*ARQM*	GCM III at Toronto	GCM	2.8 / 2.8	32	yr 2000	all	Gong
MI	*PNNL*	MIRAGE 2 at PNNL	GCM	2.5 / 2.0	24	1-yr avg	all	Ghan / Easter
EH	*MPI-HAM*	ECHAM5.2 MPI-Met	GCM	1.8 / 1.8	31	3-yr avg	all	Stier / Feichter
NF	*MATCH*	MATCH 4.2 at NCAR	CTM	1.9 / 1.9	28	yr 2000	all	Fillmore / Collins
OT	*UIO_CTM*	CTM 2 at Oslo Univ.	CTM	2.8 / 2.8	40	yr 2000	all	Myhre et al.
OG	*UIO_GCM*	CCM3.2 at Oslo Univ.	GCM	2.8 / 2.8	18	3-yr avg	all	Iversen et.al.
IM	*UMI*	IMPACT at U. Mich	CTM	2.5 / 2.0	30	yr 2000	all	Liu / Penner
GM	*MOZGN*	MOZART 2.5, GFDL	CTM	1.9 / 1.9	28	yr 2000	all	Ginoux / Horowitz
GO	*GOCART*	GOCART 3.1b, GSFC	CTM	2.0 / 2.5	30	yr 2000	all	Chin / Diehl
GI	*GISS*	Model E at GISS	GCM	4.0 / 5.0	20	yr 2000	all	Koch / Bauer
TM	*TM5*	TM5 at Utrecht	CTM	4.0 / 6.0	25	yr 2000	all	Krol / Dentener
EM	*DLR*	ECHAM 4 at DLR	GCM	3.8 / 3.8	19	10-yr avg	m	Lauer / Hendricks
GR		GRANTOUR, U. Mich	CTM	5.0 / 5.0		1-yr avg	m, aot	Herzog / Penner
NM		MOZART at NCAR	CTM	1.9 / 1.9		1-yr avg	m, aot	Tie / Brasseur
NC		CAM at NCAR	CTM	2.8 / 2.8	26	1-yr avg	all	Mahowald
EL		ECHAM4, Dalh. Univ.	GCM	3.8 / 3.8		3-yr avg	m, aot	Lesins / Lohmann

note: only models with AeroCom IDs have submitted data according to the AeroCom request
GCM – Global Circulation Model (nudging preferred), CTM – Chemical Transport Model

Table 3. Aot data-sets from remote sensing data used in comparisons to models.

	Sensor	Period	Ocean	Land	Limitation	Biases
Ae	*AERONET*	3/01–2/01+98–04	–	Holben 98	local sample	– pristine case
To	*TOMS*	79–81, 84–90, 96–99	Torres 98	Torres 98	50 km pixel size	+ + cloud cont.
Mi	*MISR*	3/00–2/01	Kahn 98	Martonchik 98	6-day repeat	+ over ocean
Mo	*MODIS*	3/00–2/01	Tanré 97	Kaufman 97	not over deserts	+ over land
Mn	*MODIS, ocean*	3/00–2/01	Tanré 97		not over land	
An	*AVHRR, 1ch*	3/00–2/01	Ignatov 02	–	no land, a-priori	– size overest.
Ag	*AVHRR, 2ch*	84–90, 95–00	Geogdzhyev 02	–	no land	+ cloud cont.
Po	*POLDER*	11/96–6/97, 4–10/03	Deuzé 99	Deuzé 01	land + large sizes	+ at high elev.

Table 4. Comparison of annual global averages for aerosol optical depth (**AOT**), aerosol dry mass (**M**) and its ratio (**ME**) for 20 aerosol component modules in global modeling.

	LO[1]	LS[1]	UL[1]	SP[1]	CT[1]	MI[1]	EH[1]	NF[1]	OT[1]	OG[1]	IM[1]	GM[1]	GO[1]	GI[1]	TM[1]	EM[1]	GR[1]	NM[1]	NC[1]	EL[1]	Med[2]	MaxMin[3]
M, mg/m^2																						
-SU[4]	**4.2**	**5.3**	**1.8**	**2.1**	**3.3**	**3.9**	**4.6**	**3.3**	**3.7**	**2.8**	**4.3**	**5.2**	**3.8**	**2.8**	**1.8**	**5.1**	2.7	4.3	4.7	3.0	**3.9**	2.9(**1.6**)
-BC[4]	**.35**	**.43**	**1.0**	**.73**	**.48**	**.37**	**.22**	**.37**	**.38**	**.36**	**.40**	**.50**	**.53**	**.44**	**.09**	**.29**	.58	.45	.45	.35	**.39**	11(**1.4**)
-POM[4]	**3.5**	**3.2**	**4.1**	**4.5**	**5.0**	**4.0**	**1.9**	**3.3**	**4.0**	**2.0**	**3.3**	**3.1**	**3.4**	**2.9**	**0.9**	**2.6**	2.3	2.8	1.4	3.7	**3.3**	5.6(**1.5**)
-DU[4]	**26.9**	**40.1**	**57.2**	**34.0**	**8.8**	**43.4**	**16.2**	**34.0**	**43.0**	**46.6**	**38.1**	**41.3**	**57.8**	**56.6**	**26.1**	**18.4**	36.2	30.4	34.6	17.7	**39.1**	6.6(**1.8**)
-SS[4]	**8.9**	**24.7**	**12.8**	**14.4**	**18.5**	**10.8**	**20.4**	**8.1**	**18.0**	**8.9**	**7.0**	**6.8**	**25.8**	**12.3**	**4.8**	**15.8**	15.0	25.9	27.5	3.0	**12.6**	5.4(**2.3**)
-total	***44***	***74***	***77***	***56***	***36***	***62***	***43***	***49***	***69***	***60***	***53***	***57***	***92***	***75***	***34***	***42***	*57*	*64*	*64*	*28*	***56***	2.7(**1.7**)
-water	***48***	***115***	***55***	***35***			***147***		***255***	***54***	***47***		***36***								***54***	7.1(**3.1**)
f^5_{MASS}	**.18**	**.12**	**.09**	**.13**	**.24**	**.13**	**.16**	**.14**	**.12**	**.09**	**.15**	**.15**	**.08**	**.08**	**.08**	**.19**	.10	.12	.10	.25	**.13**	2.9(**1.7**)
$r^5_{POM/BC}$	**10**	**7.4**	**4.1**	**6.2**	**10.4**	**10.8**	**8.6**	**8.9**	**10.5**	**5.5**	**8.3**	**6.2**	**6.4**	**6.5**	**10**	**9.0**	4.0	6.2	3.1	10.6	**8.4**	3.2(**1.6**)
AOT$_{550\,nm}$																						
-SU[4]	**.042**	**.041**	**.051**	**.034**	**.015**	**.027**	[7]	**.051**	**.041**	**.020**	**.034**	**.049**	**.032**	**.027**	**.024**		.023	.041	.047	.032	**.034**	3.4(**2.0**)
-BC[4]	**.0033**	**.0036**	**.0088**	**.0058**	**.0030**	**.0050**	[7]	**.0034**	**.0020**	**.0021**	**.0037**	**.0056**	**.0053**	**.0039**	**.0017**		.0054	.0100	.0031	.0027	**.004**	5.2(**2.7**)
-POM[4]	**.021**	**.018**	**.018**	**.030**	**.018**	**.021**	[7]	**.019**	**.024**	**.009**	**.026**	**.021**	**.011**	**.015**	**.006**		.018	.036	.014	.013	**.019**	5.0(**2.1**)
-DU[4]	**.034**	**.031**	**.040**	**.024**	**.013**	**.053**	[7]	**.033**	**.026**	**.053**	**.021**	**.021**	**.035**	**.054**	**.012**		.037	.027	.035	.009	**.032**	4.5(**2.5**)
-SS[4]	**.027**	**.034**	**.030**	**.021**	**.048**	**.030**	[7]	**.021**	**.054**	**.067**	**.031**	**.020**	**.025**	**.035**	**.021**		.048	.028	.028	.003	**.030**	3.3(**2.3**)
-total	***.127***	***.128***	***.149***	***.115***	***.097***	***.136***	***.138***	***.127***	***.148***	***.151***	***.116***	***.117***	***.108***	***.134***	***.065***		*.131*	*.142*	*.127*	*.060*	***.127***	2.3(**1.3**)
-abs	***.0037***			***.0062***			***.0020***	***.0059***	***.0044***	***.0064***	***.0028***	***.0061***							*.0067*		***.005***	3.2(**2.2**)
f^6_{AOT}	**.45**	**.48**	**.52**	**.42**	**.37**	**.30**	[7]	**.51**	**.44**	**.27**	**.45**	**.57**	**.45**	**.33**	**.49**		.35	.61	.50	.80	**.50**	**3.1**(**1.6**)
Angstrom	***0.70***			***0.68***			***0.71***	***0.63***	***0.97***	***0.86***	***0.13***	***0.48***							*1.01*		***.70***	7.4(**1.8**)
ME, m^2/g																						
SU[4]	**10.2**	**7.8**	**28.3**	**18.0**	**4.2**	**6.3**	[7]	**17.8**	**11.1**	**7.2**	**7.8**	**8.5**	**8.4**	**9.5**	**13.3**		8.9	9.2	14.5	13.0	**8.5**	6.7(**2.5**)
BC[4]	**9.4**	**8.2**	**8.8**	**8.0**	**6.5**	**13.1**	[7]	**9.2**	**5.3**	**5.7**	**9.3**	**10.4**	**10.0**	**8.9**	**18.9**		9.3	15.9	9.1	7.6	**8.9**	3.5(**1.6**)
POM[4]	**6.4**	**5.7**	**4.4**	**9.1**	**3.7**	**5.0**	[7]	**4.6**	**6.0**	**4.4**	**8.0**	**6.3**	**3.2**	**5.1**	**6.7**		8.2	11.4	3.9	5.3	**5.7**	2.8(**1.5**)
DU[4]	**1.38**	**.88**	**.70**	**1.04**	**2.05**	**1.62**	[7]	**1.07**	**.60**	**1.14**	**.68**	**.66**	**.60**	**.95**	**0.46**		1.24	.98	.99	.52	**.95**	15.(**2.3**)
SS[4]	**3.10**	**1.46**	**2.34**	**1.51**	**3.13**	**3.38**	[7]	**1.78**	**3.05**	**7.53**	**4.33**	**2.37**	**.97**	**2.84**	**4.3**		3.44	.90	.88	1.69	**3.0**	7.7(**2.9**)

[1] model abbreviations: **LO**=LOA (Lille, Fra), **LS**=LSCE (Paris, Fra), **UL**=ULAQ (L'Aquila, Ita), **SP**=SPRINTARS (Kyushu, Jap), **CT**=ARQM (Toronto, Can), **MI**=MIRAGE (Richland, USA), **EH**=ECHAM5 (MPI-Hamburg, Ger), **NF**=CCM-Match (NCAR-Boulder, USA), **OT**=Oslo-CTM (Oslo, Nor), **OG**=OLSO-GCM (Oslo, Nor) (prescribed background for DU and SS), **IM**=IMPACT (Michigan, USA), **GM**=GFDL-Mozart (Princeton, NJ, USA), **GO**=GOCART (NASA-GSFC, Washington DC, USA), **GI**=GISS (NASA-GISS, New York, USA), **TM**=TM5 (Utrecht, Net), **EM**=ECHAM4 (DLR, Oberpfaffenhofen, Ger) [Exp B-data], GR=GRANTOUR (Michigan, USA), NM=CCM-Mozart (NCAR-Boulder, USA), NC=CCM-CAM (NCAR-Boulder, USA), EL=ECHAM4 (Dalhousie, Can) (bold letters indicate models participation in the AeroCom exercise)

[2] most likely value in modeling: global annual average of the median-ranked model (only the first 16 models participating in the AeroCom excercise are considered)

[3] model diversity indicators: ratio of the maximum global annual average and the minimum global annual average among all AeroCom models (first value) and among remaining AeroCom models, after models with the two largest and smallest averages were removed (second value in brackets)

[4] aerosol component abbreviations: SU=sulfate, BC=black carbon, POM= particulate organic matter (↔1.4*OC, OC=organic carbon), DU=mineral dust, SS=sea-salt.

[5] fine-mode fraction of the total for aerosol dry mass (**MASS**) and aerosol optical depth (**AOT**), where the fine-mode here is approximated by contributions of only SU, BC and POM

[6] dry mass ratio between particulate organic matter (POM [↔1.4*OC]) and black carbon (BC)

[7] component values for aerosol optical thickness (**AOT**) and mass extinction efficiency (**ME**) for the EH-model cannot be accurately due to internal mixing of components

Table 5. AERONET references for monthly statistics of mid-visible aot and absorption aot.

AERONET-site	Location	Representing	Notables
Abracos Hill	298E / 11S	S. America	biomass: Aug-Nov
Anmyon	126E / 37N	E. Asia	Asian dust: spring
Cape Verde	337E / 17N	Off N. Africa	dust off Africa
GSFC	283E / 39N	N. America, east	sub-urban, eastern US
Lille	3E / 51N	Europe	urban, Europe
Maricopa	248E / 33N	N. America, west	rural, western US
Mongu	23E / 15S	S. America	biomass: Aug-Nov
Ouagadogou	359E / 12N	N. Africa	dust, biomass: Nov-Jan
Nes Ziona	35E / 32N	Asia	dust, rural
Rimrock	243E / 46N	N. America, west	rural , nw-USA
Stennis	270E / 30N	N. America, south	urban, maritime
Tahiti	210E / 18S	Pacific	maritime

Table 6. Regional aot averages of the model median (med) and of remote sensing data from ground (*Ae*) and space (*To, Mi, Mo, Ag, An, Po*). Individual space-sensors have different regional aot retrieval capabilities, as best agreements to ground remote sensing (*Ae*) are highlighted. Based on regional strengths of individual aot retrievals a satellite composite (S*) was formed.

	zonal reg	surface		%	med	*Ae*	S*	*To*	*Mi*	*Mo*	*Ag*	*An*	*Po*
	global	*All*	%	100.0	**.122**	*.135**	**.151***	*.220**	*.189*	*.182**	*.172**	*.138**	*.143**
1	50–90N	*ocean*	47	5.53	**.106**	*.076**	**.089***	*.234**	*.130**	*.126**	*.139**	***.077****	*.097**
2	50–90N	*Land*	53	6.16	**.112**	*.102**	**.114***	*.223**	***.109****	*.149**	*.154**	*.074**	*.083**
3	30–50N	*ocean*	45	5.98	**.148**	*.122**	**.131**	*.224**	*.238*	*.177**	*.165*	***.130***	*.154**
4	30–50N	*coast*	19	2.51	**.222**	*.173**	**.195**	*.277**	*.231*	*.287**	*.212**	*.153**	*.144**
5	30–50N	*Land*	36	4.81	**.200**	*.155**	**.206**	*.240**	***.206***	*.321**	*no data*	*no data*	*.151**
6	8–30N	*ocean*	61	10.95	**.128**	*.109**	**.177**	*.208**	*.220*	***.178****	*.159*	*.146*	*.173**
7	8–30N	*coast*	15	2.75	**.204**	*.199**	**.280**	*.351*	*.297*	*.324*	*.231**	*.217**	*.218**
8	8–30N	*land*	24	4.34	**.348**	*.377**	**.333**	*.358*	***.330***	*.448**	*no data*	*no data*	*.240**
9	8N–25S	*ocean*	70	19.75	**.079**	*.131**	**.133**	*.197*	*.179*	***.134****	*.139*	*.119*	*.146**
10	8N–25S	*coast*	13	3.50	**.106**	*.200**	**.207**	*.337*	*.258*	*.228*	*.206**	*.160**	*.199**
11	8N–25S	*land*	17	4.83	**.136**	*.194**	**.252**	*.282*	*.243*	***.248***	*no data*	*no data*	*.172**
12	25–55S	*ocean*	87	17.28	**.095**	*.060**	**.111**	*.204**	*.167*	*.132**	*.140*	***.101***	*.103**
13	25–55S	*coast*	6	1.18	**.080**	*.103**	**.106**	*.221*	*.124*	*.136**	*.123**	*.082**	*.081**
14	25–55S	*land*	7	1.36	**.086**	*.075**	**.098**	*.181**	***.098***	*.148**	*no data*	*no data*	*.112**
15	55–90S	*ocean*	70	6.31	**.088**	*no data*	**.076***	*.158**	*.138**	*.106**	*.148**	*.070**	*.064**
16	55–90S	*land*	30	2.73	**.018**	*no data*	**no data**	*.143**	*.201**	*.051**	*no data*	*no data*	*.024**

note: a * indicates a spatial sampling correction with the aot field of the model median

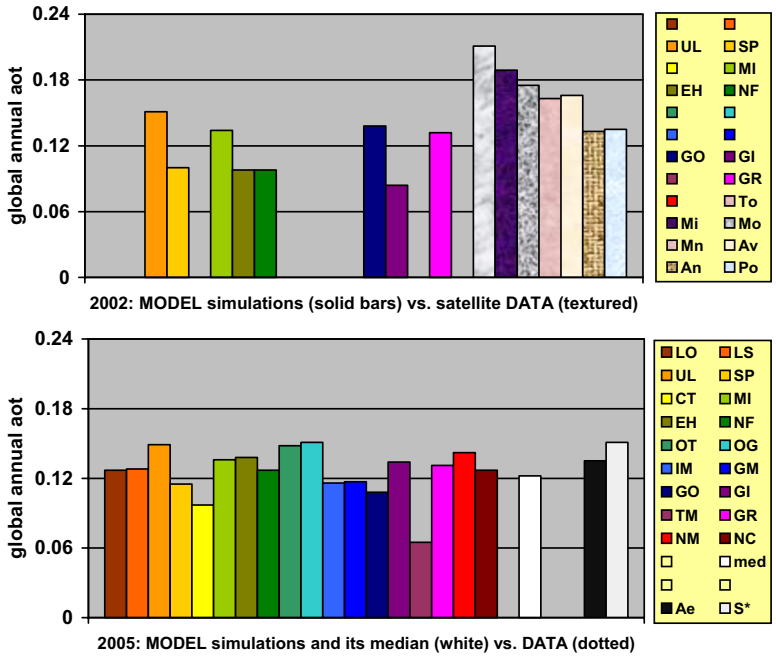

Fig. 1. Comparison for the annual global average aerosol optical thickness at .55 μm (aot) between simulations in global modeling and data derived from remote sensing measurements. The upper panel shows diversity in 2002 among models and satellite data (Kinne et al., 2003). The lower panel displays model diversity in 2005 and compares the model median to two data references from remote sensing: AERONET (Ae) and a satellite-data composite (S*). Spatial deficiencies of remote sensing data-sets in both panels have been corrected with the bias, such sub-sampling would introduce to the model median value.

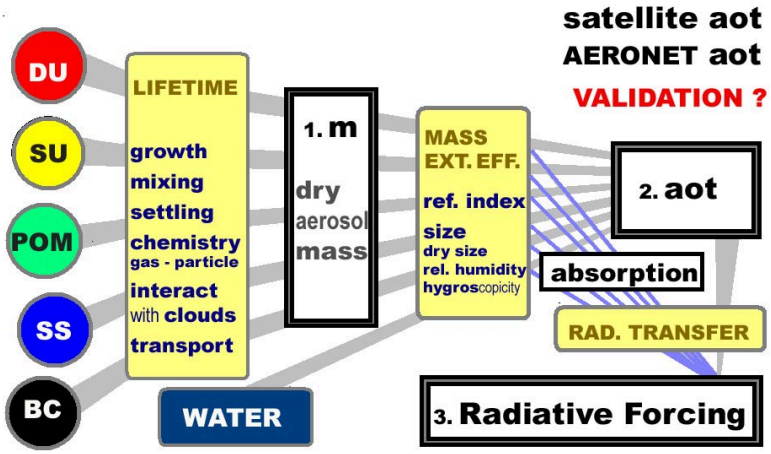

Fig. 2. An illustration of modeling steps in aerosol components modules of global models – from emissions (-fluxes) by dust (DU), sulfate (SU), particulate organic matter (POM), sea-salt (SS) and black carbon (BC), via predictions for dry mass (m) and aerosol optical thickness (aot) to estimates of climatic impacts (radiative forcing).

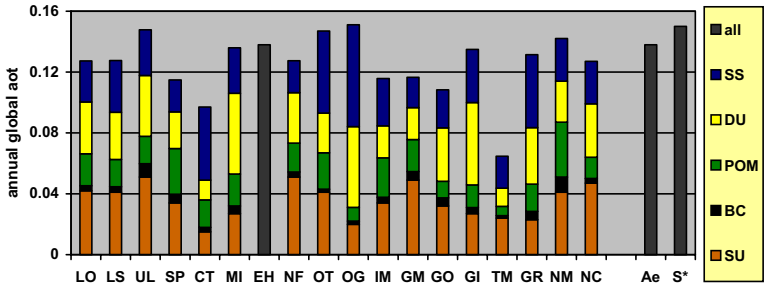

Fig. 3. Individual contributions of the five aerosol components (SS-seasalt, DU-dust, POM-particulate organic matter, BC-black carbon, SU-sulfate) to the annual global aerosol optical thickness (at 550 nm). For comparison, two 'quality' aot data references from remote sensing are provided: ground data from AERONET and a satellite-composite based on MODIS (ocean) and MISR (land) data. (No apportioning is possible for 'EH', due to inter-component mixing).

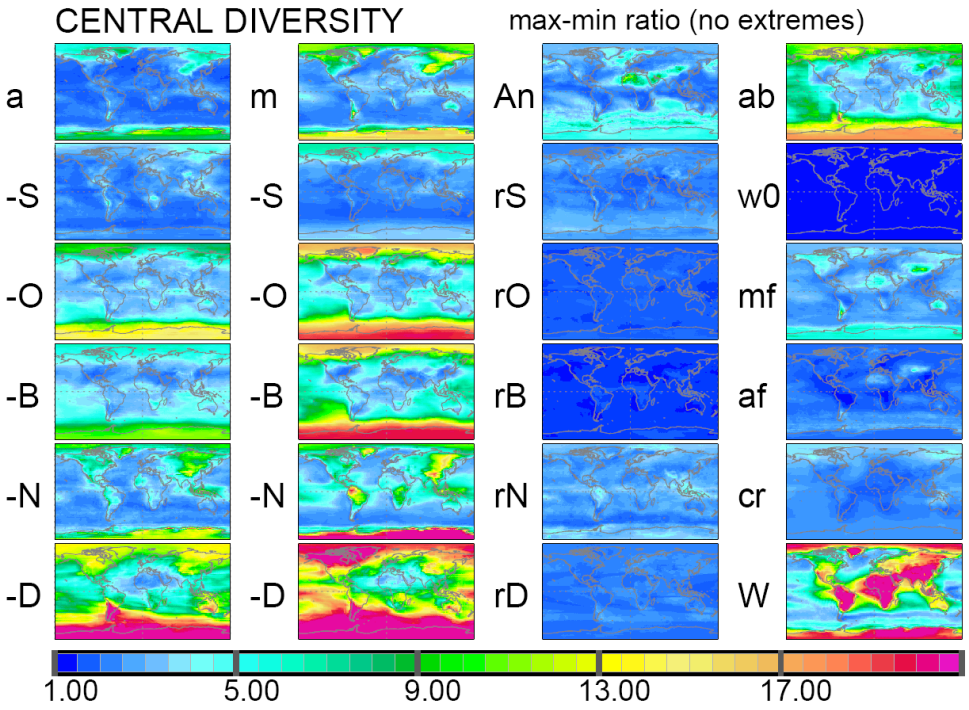

Fig. 4.

Fig. 4. Global fields for central diversity CD (max/min ratios of the central 2/3 in modeling) for yearly averages (of 16 AeroCom models). Blue colors indicate better agreement among models, while colors towards yellow or red represent significant local diversity. The left two columns present central diversity fields for aot (a) and dry mass (m): The top row displays the (sub-component combined) totals, whereas the five lower rows display the diversity separately for the five sub-components (S: sulfate, O: particulate organic matter, B: black carbon, N: seasalt, D: dust). The two right columns present diversity fields related to aerosol size (An: Angstrom parameter; mf: mass ratio between fine mode aerosol (S+O+B) and total, af: aot ratio between fine mode aerosol (S+O+B) and total, r-: mass-to-aot conversion factors for all five subcomponents), to aerosol absorption (ab: absorption aot, w0: single scattering albedo), to carbon composition (cr: POM/BC mass ratio) and to aerosol water (W).

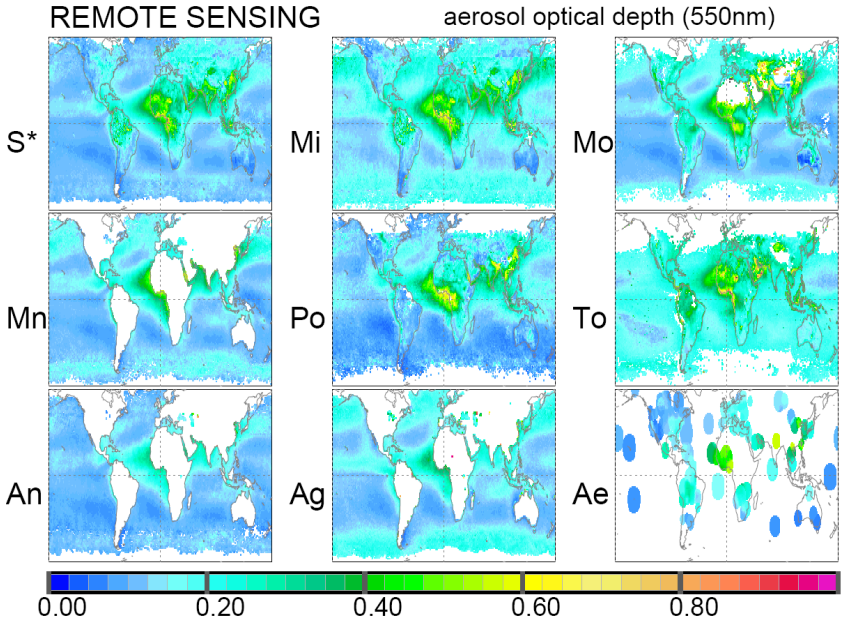

Fig. 5. Comparison of annual global fields for the mid-visible (.55 μm) aerosol optical depth from remote sensing. Retrievals of five different satellite sensors are compared: Mo, Mn – MODIS (3/00–2/01), Mi- MISR (3/00–2/01), To- TOMS (79–81, 85–90, 96–99), Po- POLDER (11/96–6/97), An- AVHRR, 1ch (3/00–2/01), Av- AVHRR, 2ch (84–90, 95–01). The satellite composite (S*) prioritizes year 2000 data. Over oceans Mn is preferred in the tropics and An is preferred at high latitudes. Over land Mi is preferred except for the tropical biomass belt (8° N–25° S), where Mo is the first choice. For comparison, year 2000 aot data of the AERONET sun photometer robotic network are presented and artificially expanded for better visualization.

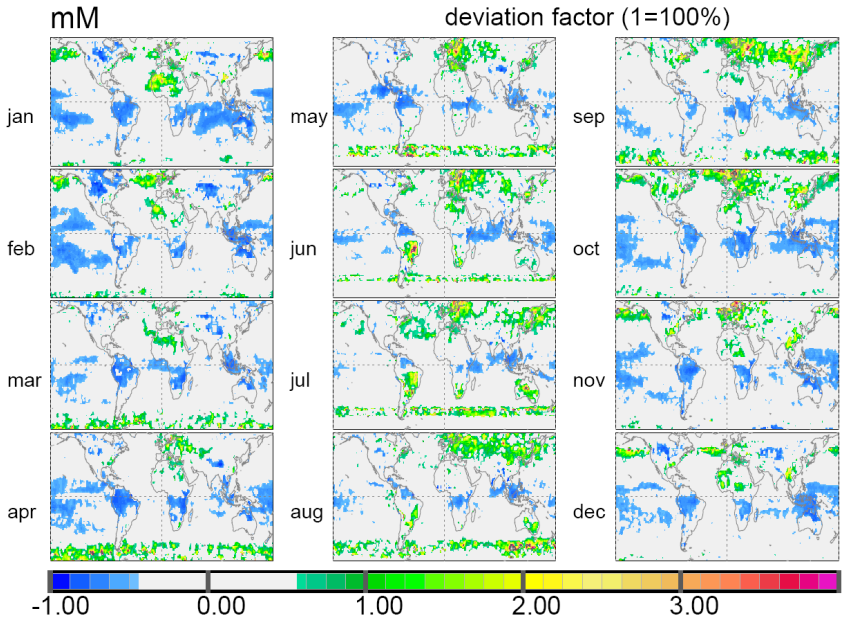

Fig. 6. Local relative deviations for aot of the (16 AeroCom) models median with respect to the satellite composite (S*) of Fig. 5 on a monthly basis. In light of satellite retrieval errors, only the more meaningful model deviations are indicated. Locations, where the model median is more than −50% below satellite suggested values are marked by blue colors, and locations, where satellite suggested values are exceeded by at least 50%, are marked in green (to red).

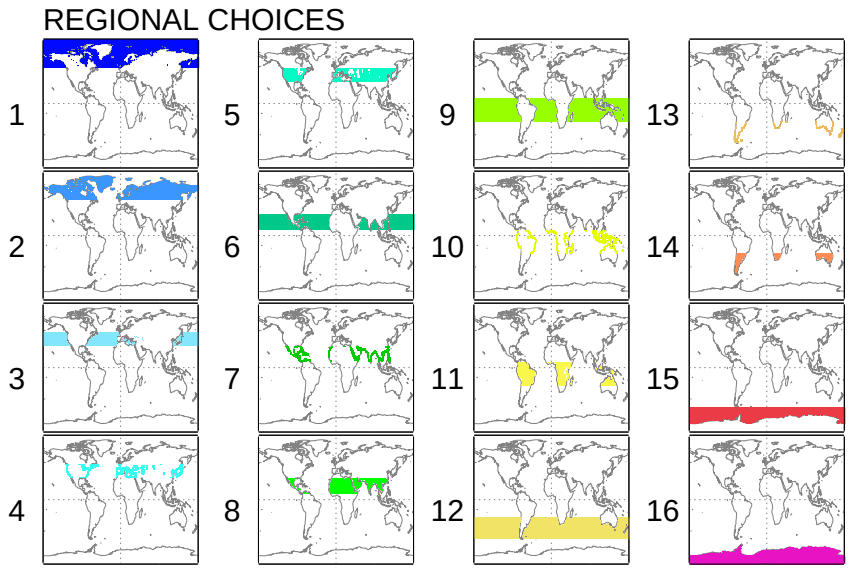

Fig. 7. Regional choices for aot-comparison among modeling and remote sensing. A distinction was made between land- ocean- and costal surfaces for selected zonal bands.

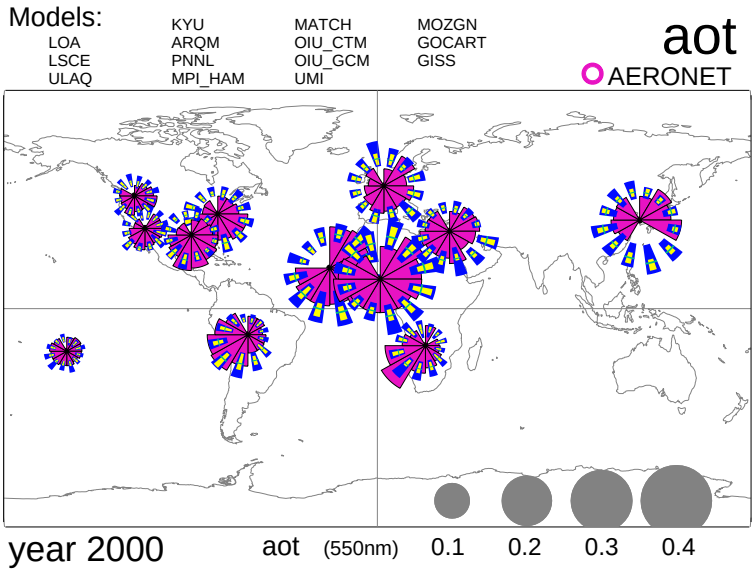

Fig. 8. Comparisons of monthly average mid-visible aot data between local statistics at AERONET sites (of Table 4) and model simulations. Monthly data are presented in a clock-hourly sense (12–1: January, 1–2: February, , 11–12: December). Purple pie disk sections indicate AERONET data according to the grey disks in the lower right. For (locally interpolated) simulations (of models listed on top) at the same scale, green lines indicate averages, maximum-minimum ranges among all models are in blue and those of just the central 2/3 models are in yellow.

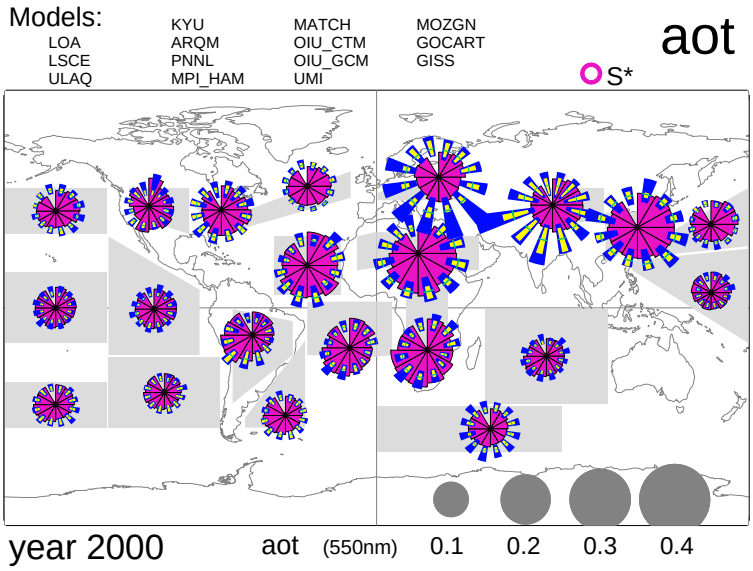

Fig. 9. Comparisons of mid-visible aot data between the satellite retrieval composite (see S* in Fig. 5) and simulations for 21 high-lighted regions. (Symbols are explained in Fig. 8.)

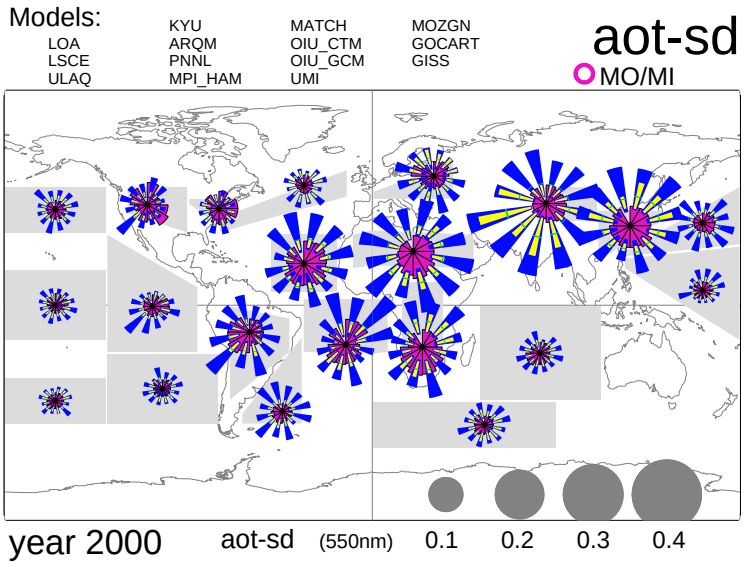

Fig. 10. Comparisons of mid-visible aot intra-regional standard deviation between the satellite retrieval composite (S* in Fig. 5) and simulations within 21 high-lighted regions. (Symbols are explained in Fig. 7).

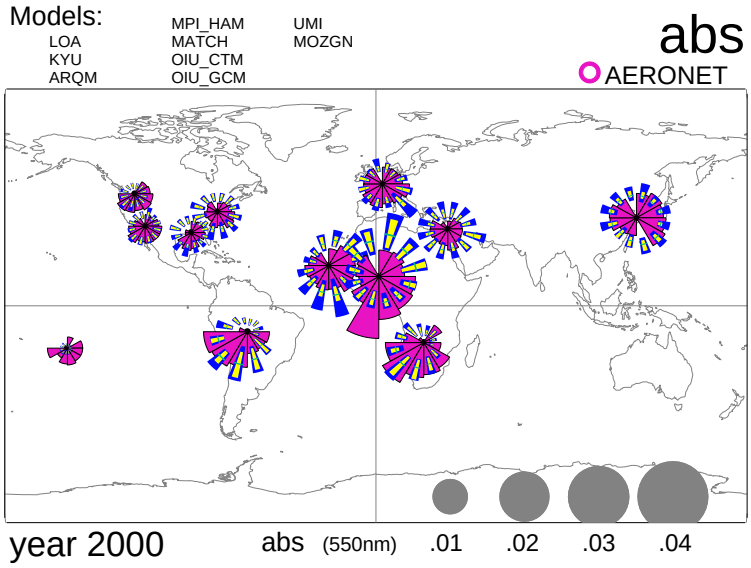

Fig. 11. Comparisons of monthly mean mid-visible absorption (aerosol) optical depth [aot*(1-ϖ0)] between local statistics at AERONET sites (of Table 5) and model simulations. (Symbols are explained in Fig. 8).

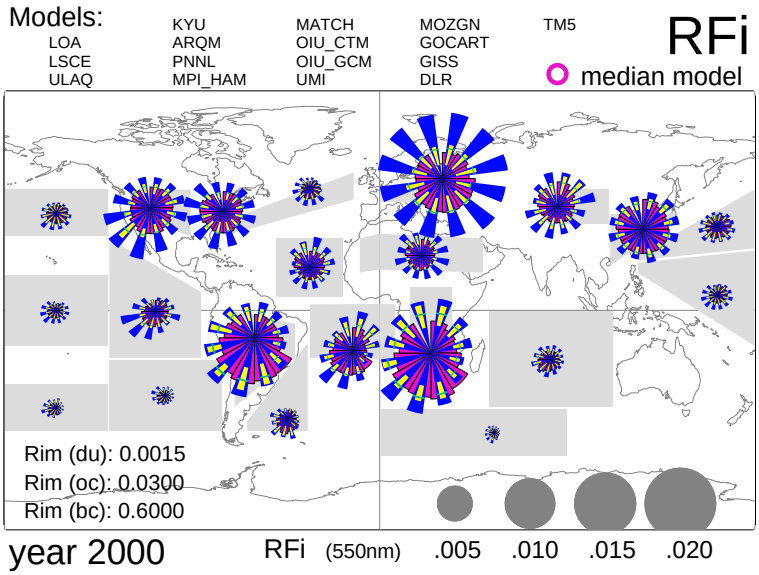

Fig. 12. Model inter-comparisons of mid-visible refractive index imaginary parts (models listed on top) on a regional basis. Estimates are based on dry mass volume weights, model median aerosol water and prescribed dry component imaginary parts: They are .0015, .03 and .6, for dust, particulate organic matter and black carbon, respectively and zero for sea-salt and sulfate. Monthly data are shown in a clock-hourly sense (12–1: January, 1–2: February, . . . , 11–12: December). The model median is purple, the average is green and simulation-ranges are blue (all models) or yellow (central models).

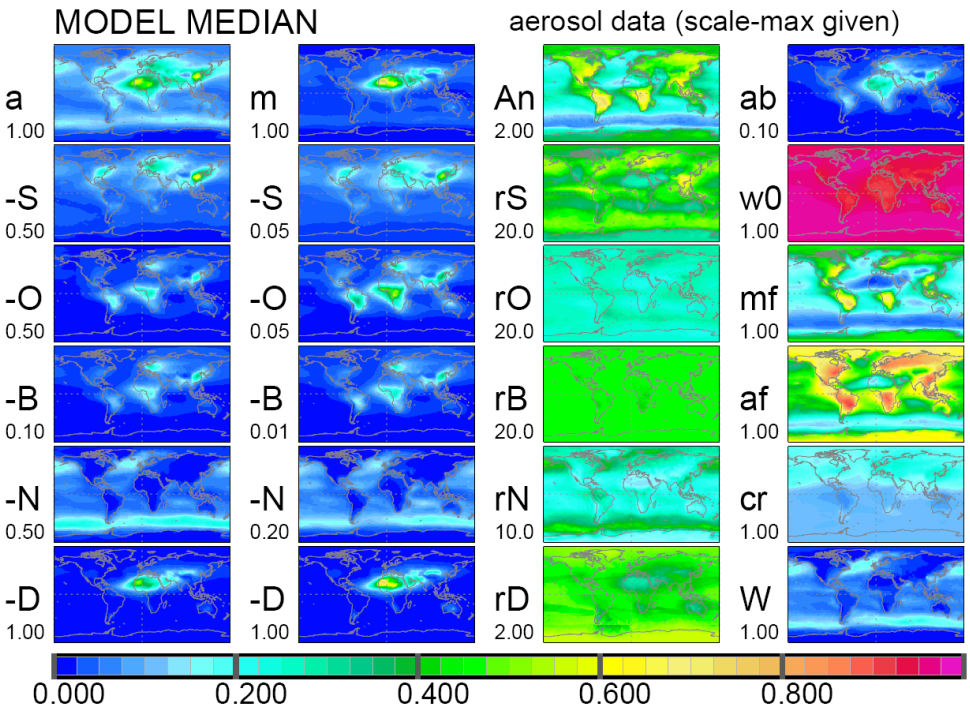

Fig. A1. Annual median fields of global modeling for aerosol properties of Fig. 4. The maximum value for the linear scale is given at the lower left of each panel. Mass (aerosol dry mass [m, -S, -O, -B, -N, -D] in the 2nd column and aerosol water [W] in the lower right corner) are given in units of g/m^2 and the mass-to-aerosol conversion (mass extinction efficiencies [r] in the 3rd column) are given in units of m^2/g. All other properties are without units.

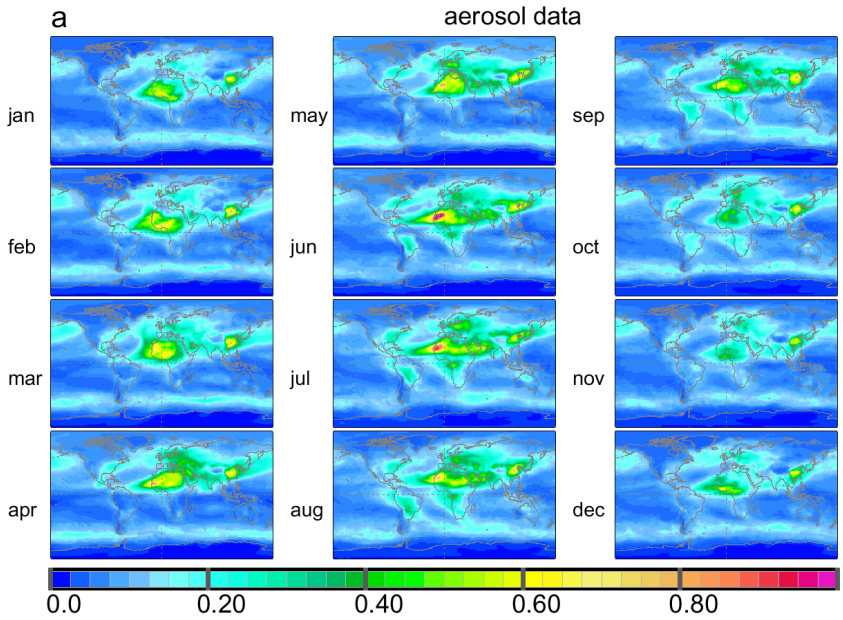

Fig. A2. Monthly median fields in global modeling for the mid-visible aerosol optical depth.

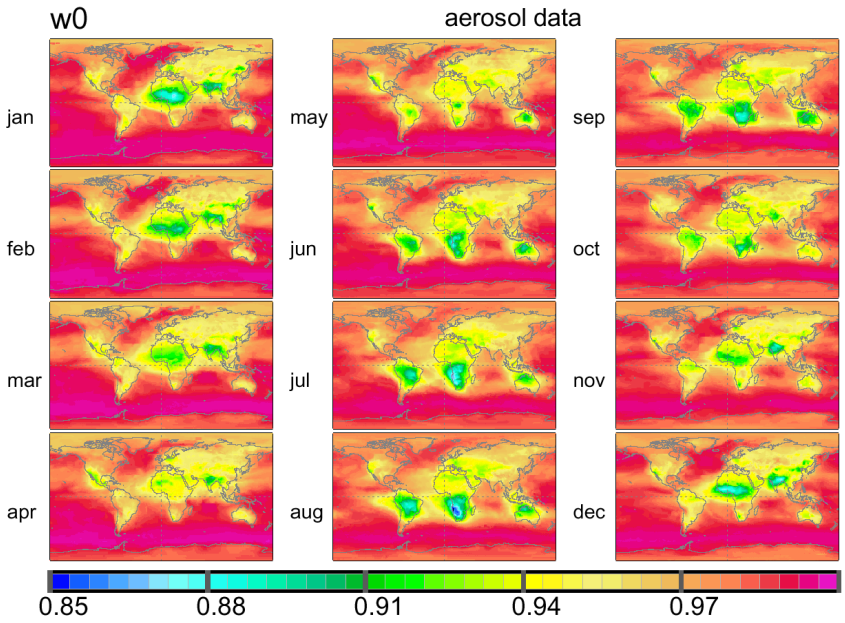

Fig. A3. Monthly median fields in global modeling for the mid-visible aerosol single scattering albedo.

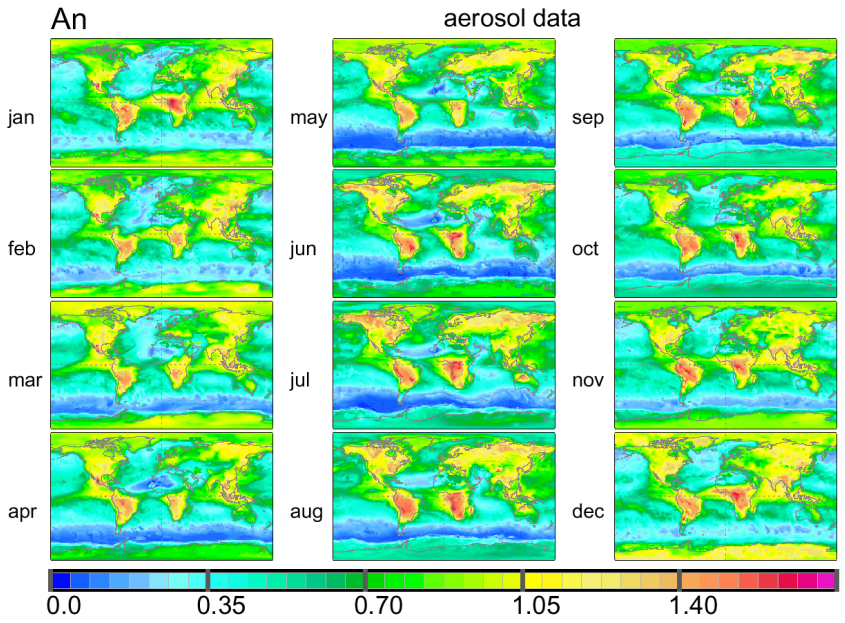

Fig. A4. Monthly median fields in global modeling for the Angstrom parameter based on simulated aerosol optical depths in the mid-visible (0.55 mm) and in the near-IR (0.865 mm).

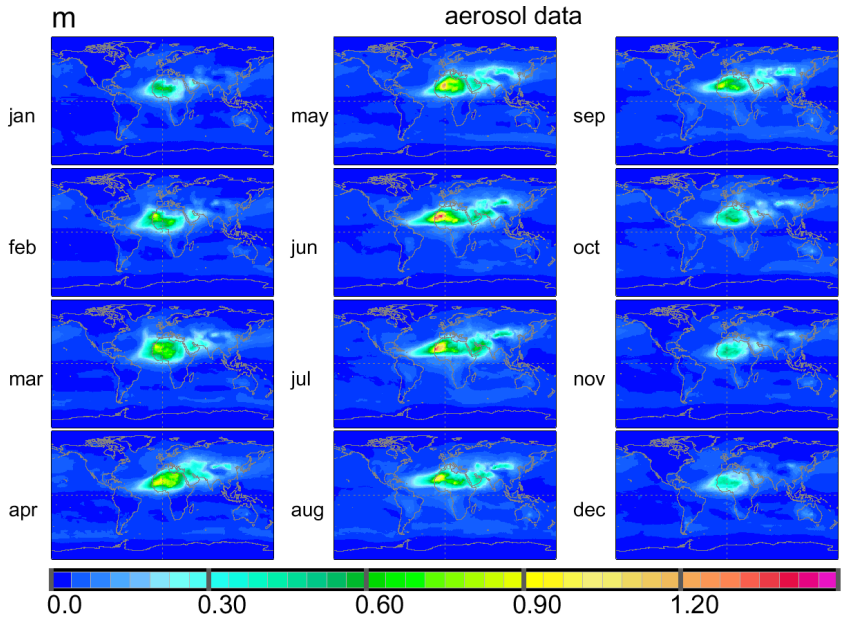

Fig. A5. Monthly median fields in global modeling for aerosol mass in g/m^2. (Mass is dominated by larger particles, thus mainly reflecting distributions of dust and sea-salt.)

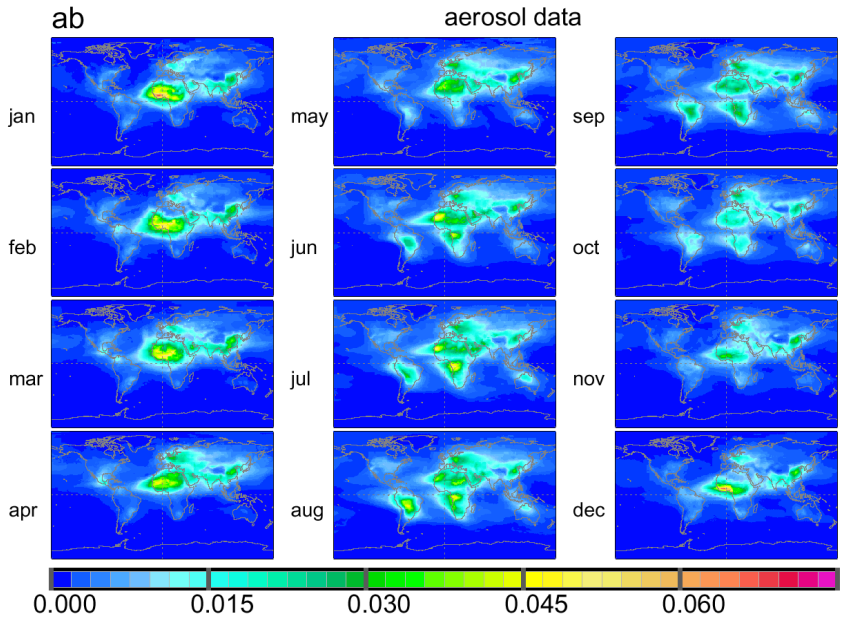

Fig. A6. Monthly median fields in global modeling for aerosol absorptions based on simulated aerosol optical depth and single scattering albedo fields of Figs. A2 and A3.